Supporting Information (SI) for:

Combined Experimental and Theoretical Investigation of the Origin of Magnetic Anisotropy in Pentagonal Bipyramidal Isothiocyanato Co(II), Ni(II) and Fe(III) Complexes With Quaternary Ammonium-functionalized 2,6-diacetylpyridine Bisacylhydrazone

Darinka Darmanović[†], Igor N. Shcherbakov[‡], Carole Duboc[§], Vojislav Spasojević[||], Darko Hanžel[⊥], Katarina Anđelković[†], Dušanka Radanović[#], Iztok Turel[▽], Milica Milenković[†], Maja Gruden[†], Božidar Čobeljić[†] and Matija Zlatar*[#]*

[†]Faculty of Chemistry, University of Belgrade, Studentski trg 12-16, 11000 Belgrade, Serbia

[‡]Faculty of Chemistry, Southern Federal University, Zorge 7, 344090, Rostov-on-Don, Russia

[§] Univ. Grenoble Alpes, CNRS, DCM, 38000 Grenoble, France

[||]Institute of Nuclear Sciences 'Vinča', Condensed Matter Physics Laboratory, P.O. Box 522, 11001 Belgrade, Serbia

[⊥]Jozef Stefan Institute, Jamova 39, SI-1000 Ljubljana, Slovenia

[#]Department of Chemistry, Institute of Chemistry, Technology and Metallurgy, National Institute, University of Belgrade, Njegoševa 12, 11000 Belgrade, Serbia.

[▽]Faculty of Chemistry and Chemical Technology, University of Ljubljana, Večna pot 113, 1000, Ljubljana, Slovenia

*Corresponding Authors: bozidar@chem.bg.ac.rs; matijaz@chem.bg.ac.rs

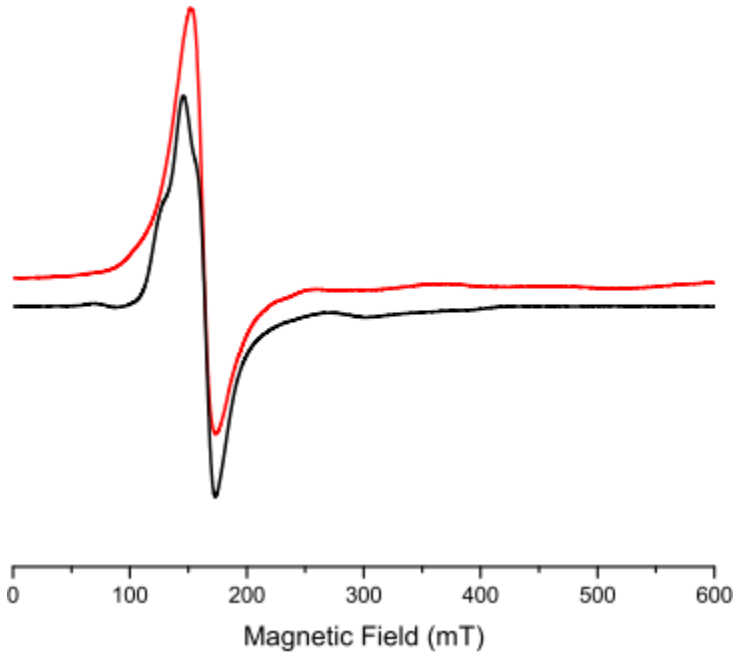

Figure S1: Powder X-band EPR spectra of complexes 1 (red line) and 2 (black line).

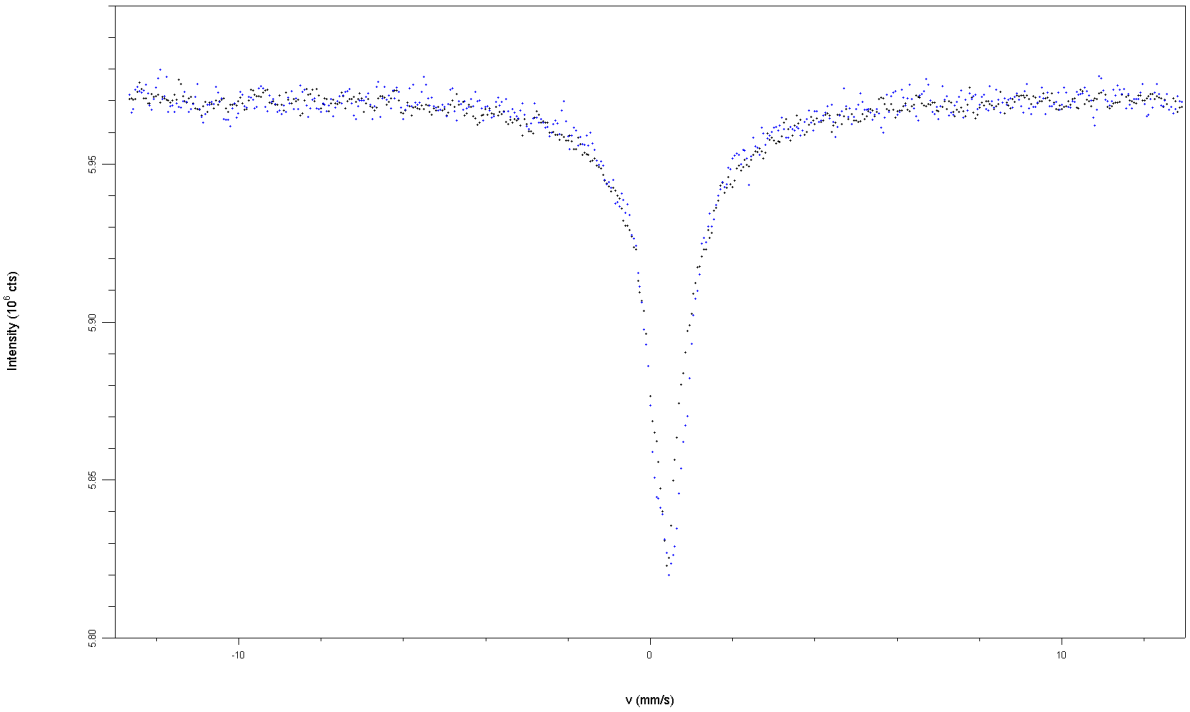

Figure S2: Comparison of normalized ^{57}Fe Mössbauer spectra of Complex **3** (black dots) and Complex **4** (blue dots) recorded at 295K

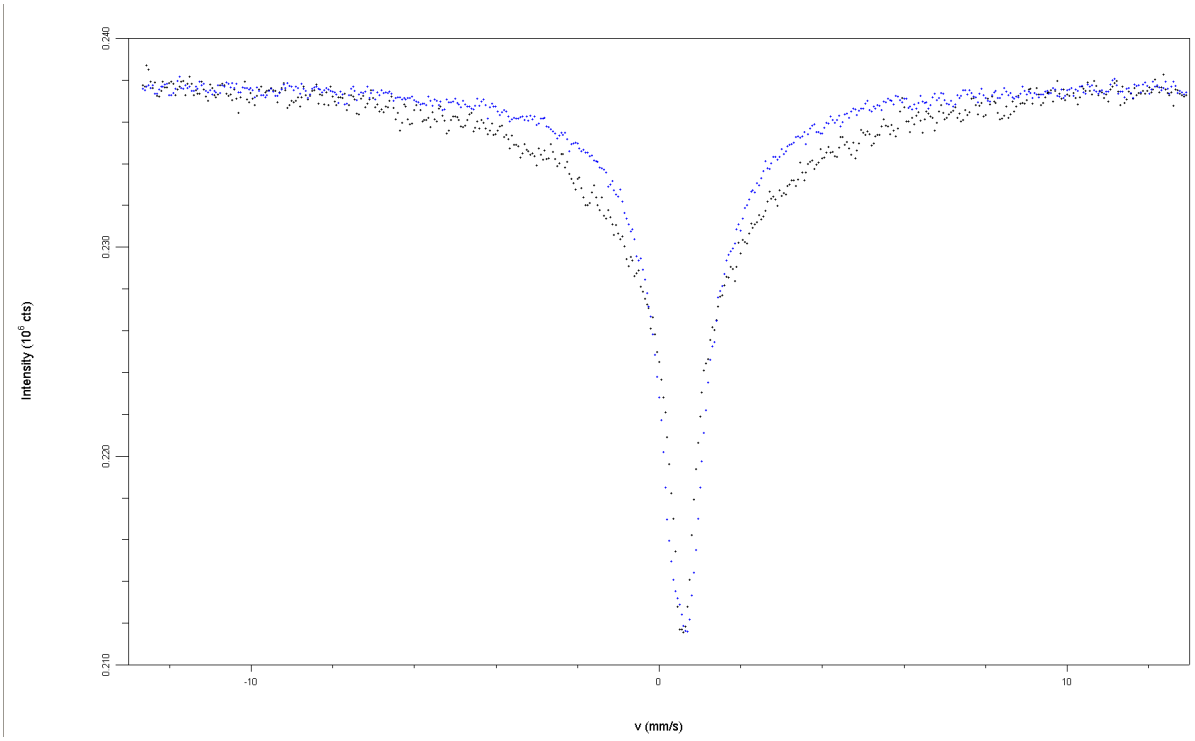

Figure S3: Comparison of normalized ^{57}Fe Mössbauer spectra of Complex **3** (black dots) and Complex **4** (blue dots) recorded at 4K

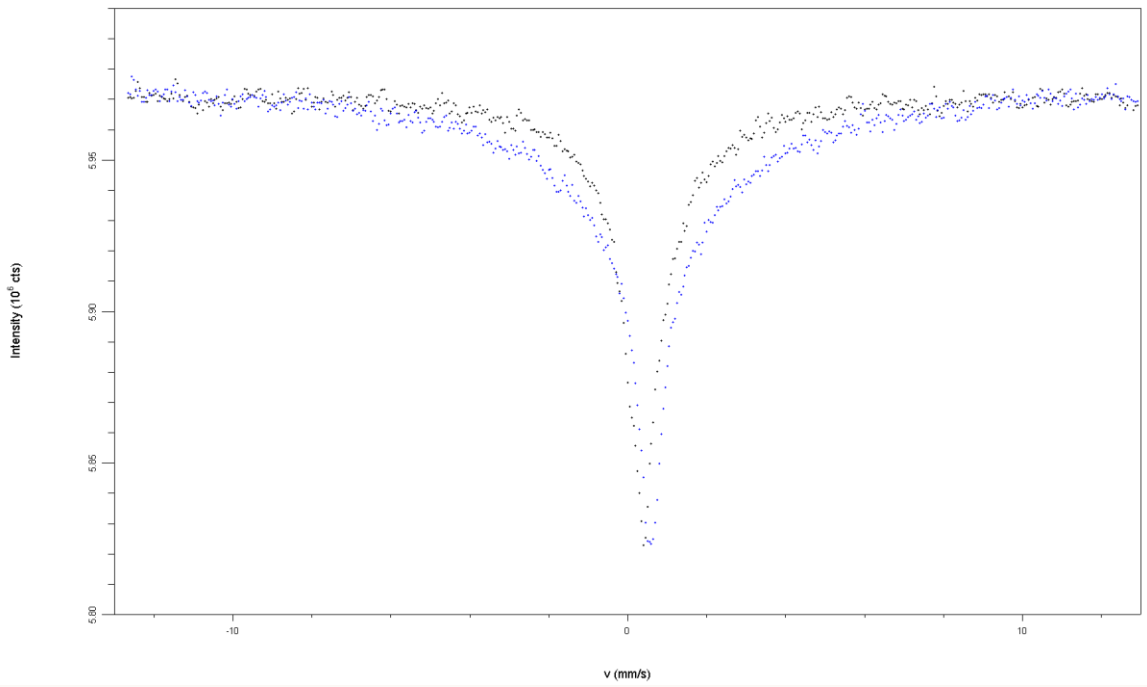

Figure S4: Comparison of normalized ^{57}Fe Mössbauer spectra of Complex **3** recorded at 295K (black dots) and recorded at 4K (blue dots)

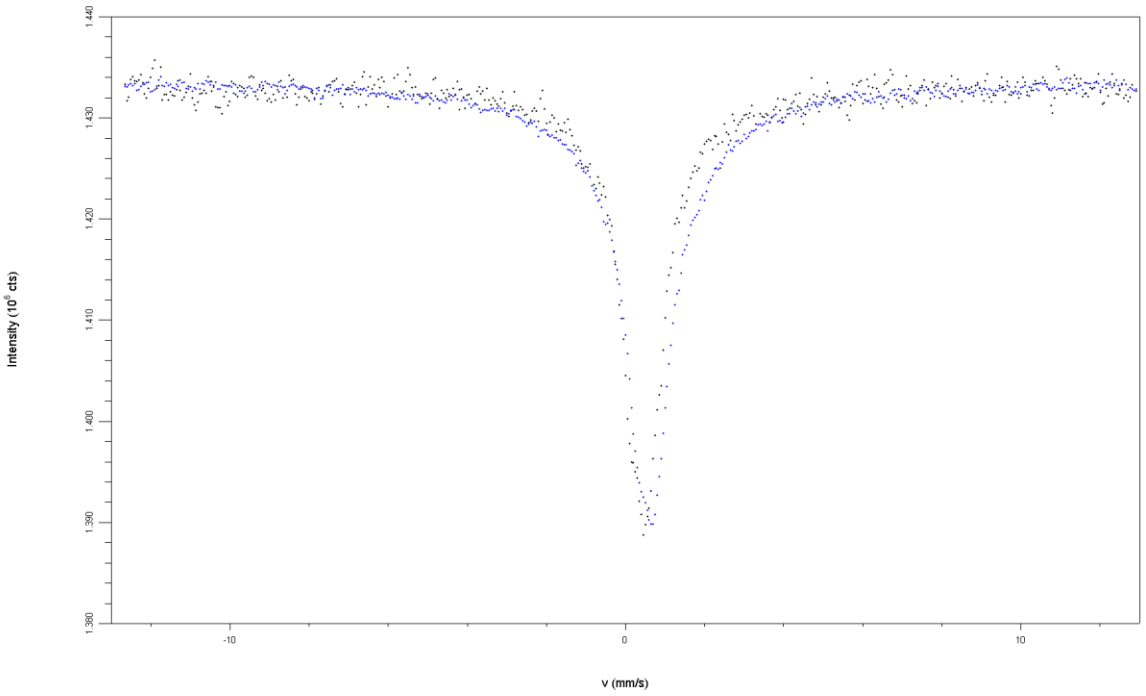

Figure S5: Comparison of normalized ^{57}Fe Mössbauer spectra of Complex 4 recorded at 295K (black dots) and recorded at 4K (blue dots)

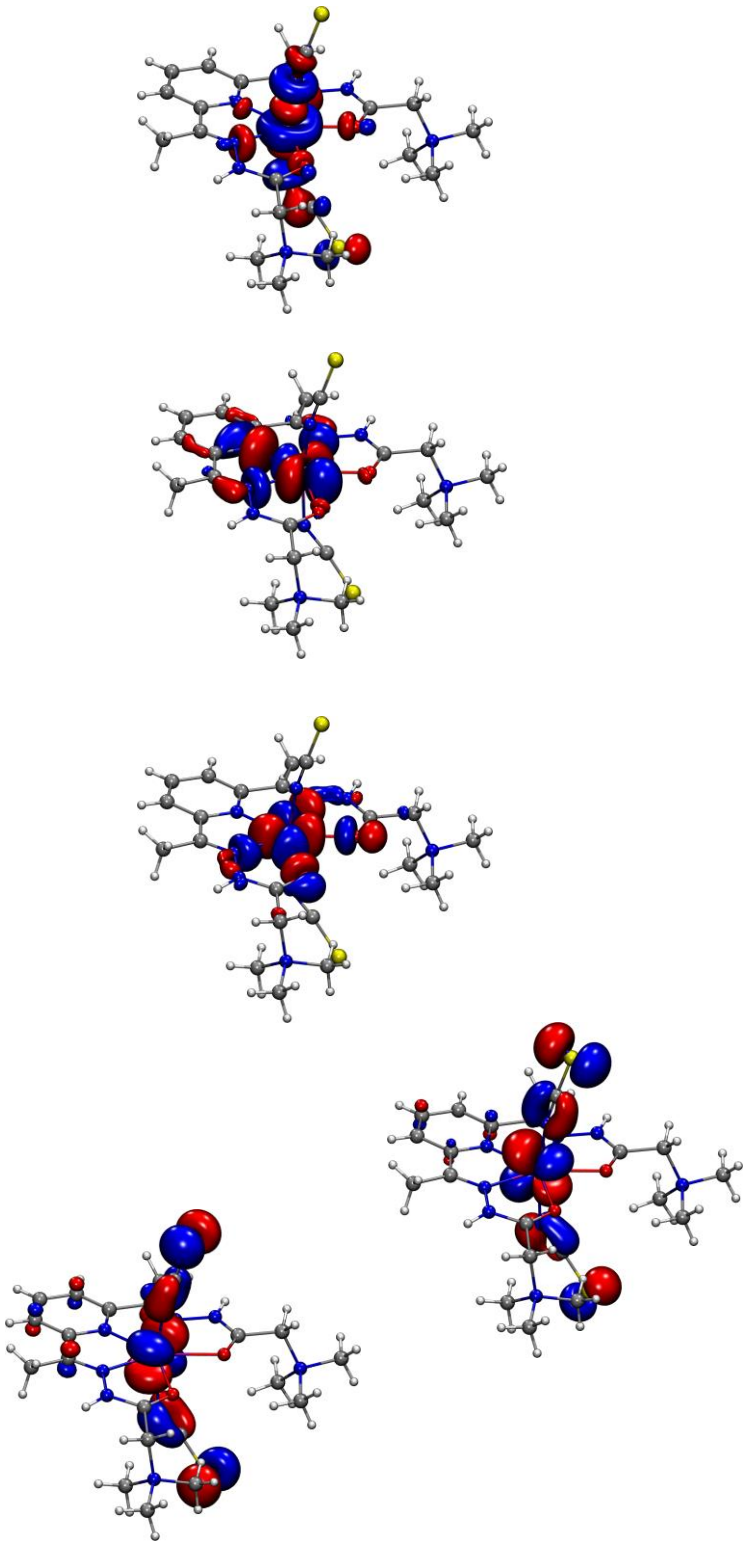

Figure S6 Kohn-Sham molecular orbitals with dominant metal d character for Co(II) complex **1** (iso-value 0.03 a.u.) generated in an average of configuration (AOC) calculations at ZORA-OPBE(COSMO-water)/TZP level of theory

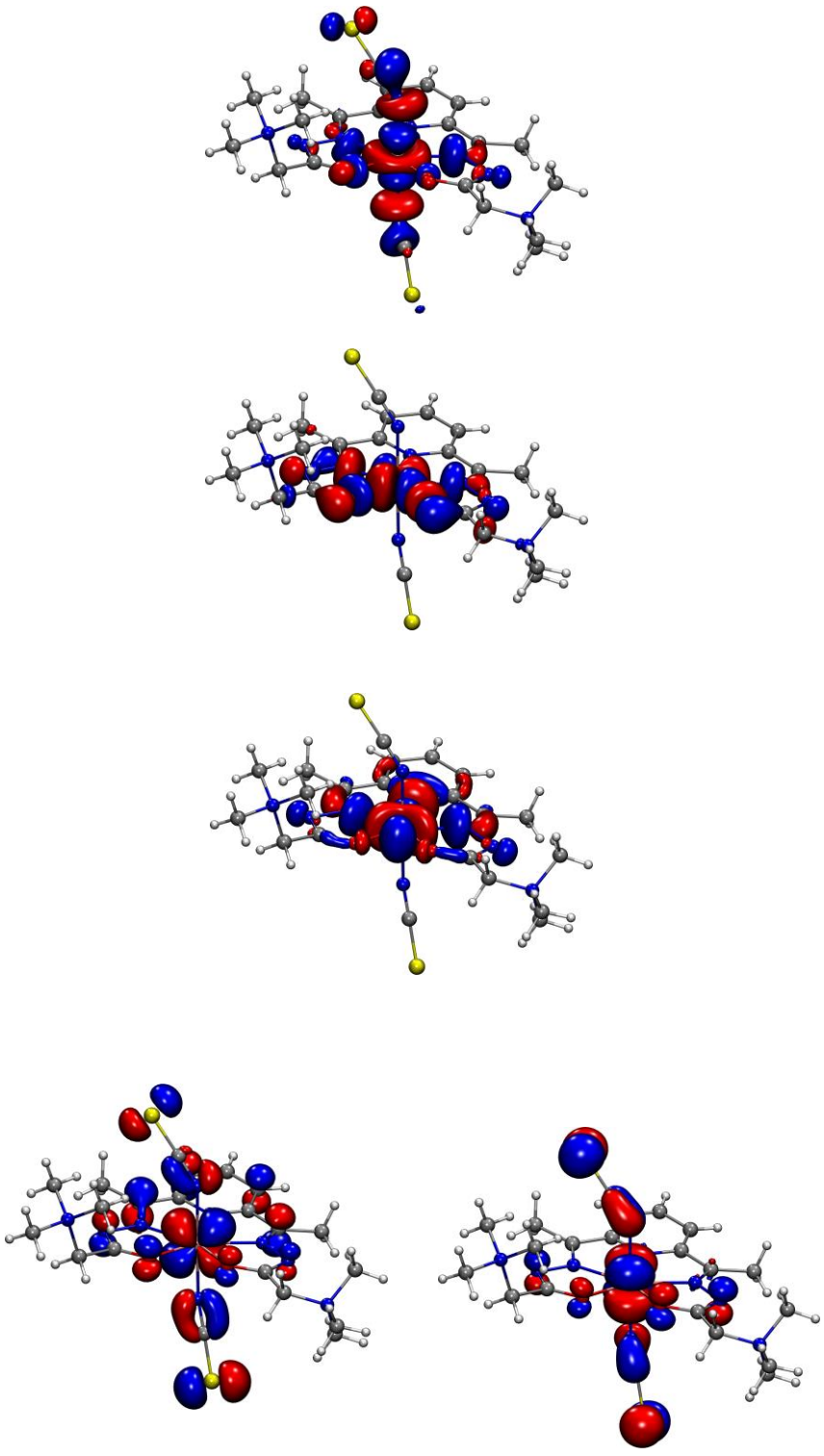

Figure S7 Kohn-Sham molecular orbitals with dominant metal d character for Fe(III) complex **3** (iso-value 0.03 a.u.) generated in an average of configuration (AOC) calculations at ZORA-OPBE(COSMO-water)/TZP level of theory

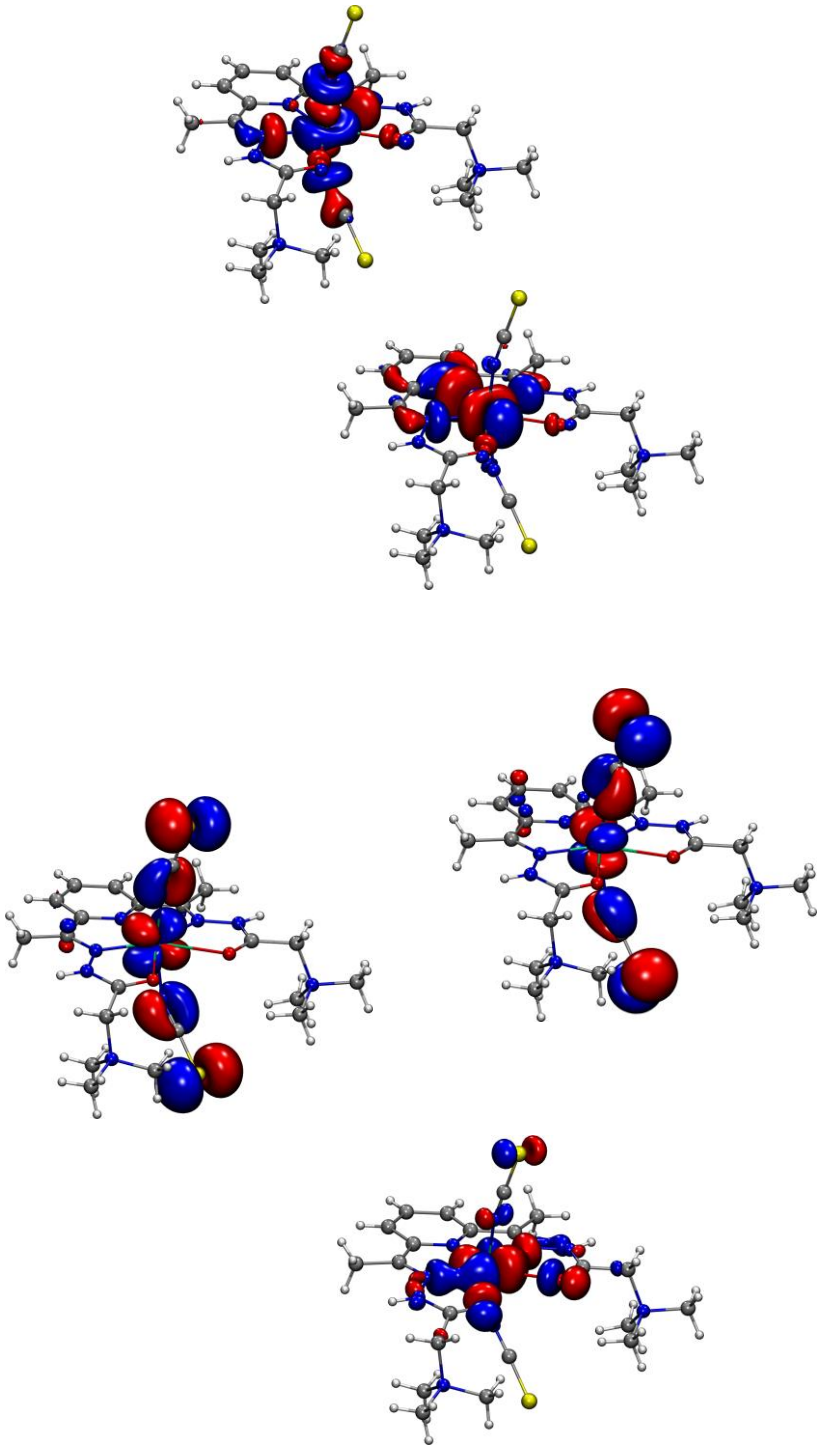

Figure S8 Kohn-Sham molecular orbitals with dominant metal d character for Ni(II) complex **5** (iso-value 0.03 a.u.) generated in an average of configuration (AOC) calculations at ZORA-OPBE(COSMO-water)/TZP level of theory

Table S1 Calculated principal components of g-tensor within CASSCF+NEVPT2 approach for PBPY-7 **1-5** compounds

Complex	M	g_x	g_y	g_z	g_{iso}
1	Co(II)	1.994	2.371	2.415	2.260
2	Co(II)	1.999	2.336	2.362	2.233
3	Fe(III)	2.000	2.000	2.000	2.000
4-1*	Fe(III)	2.002	2.002	2.002	2.002
4-2*	Fe(III)	2.002	2.002	2.002	2.002
5	Ni(II)	2.224	2.266	2.343	2.278

*Two independent heptacoordinated Fe(III) species were calculated

Table S3. Comparison of calculated (BS-DFT) and experimental magnetic exchange coupling between paramagnetic centers in **2** and **4**; values are given in cm^{-1}.

	$J_{PBPY7\text{-}T4}$ (**2**)	$J_{PBPY7\text{-}PBPY7}$ (**4**)	$J_{PBPY7\text{-}OC6}$ (**4**)
Exp.	-0.02	-0.02	-0.03
Calc.	-0.08	-0.02	-0.21

The exchange coupling constant *J* was calculated within broken symmetry DFT formalism[1–5] according to the Yamaguchi approach.[6] All calculations were performed with the ORCA program package (version 4.0.1.2) using increased integration grids (Grid5). Scalar relativistic effects were considered at the ZORA level. B97-D functional,[7] proven to be good for this problem,[8] and ZORA-def2-TZVP basis set for all atoms have been used. The resolution of the identity (RI) approximation in the Split-RI-J variant with the scalar relativistically recontracted SARC/J Coulomb fitting sets has been used. CPCM(water) model was employed in order to approximately simulate the environmental effects in the crystal lattice of charged complexes.[9]

(1) Jonkers, G.; de Lange, C. A.; Noodleman, L.; Baerends, E. J. Broken symmetry effects in the He(I) valence photoelectron spectrum of Se(CN) $_2$. *Mol. Phys.* **1982**, *46* (3), 609–620 DOI: 10.1080/00268978200101431.

(2) Noodleman, L. Valence bond description of antiferromagnetic coupling in transition metal dimers. *J. Chem. Phys.* **1981**, *74* (10), 5737–5743 DOI: 10.1063/1.440939.

(3) Noodleman, L.; Davidson, E. R. Ligand spin polarization and antiferromagnetic coupling in transition metal dimers. *Chem. Phys.* **1986**, *109* (1), 131–143 DOI: 10.1016/0301-0104(86)80192-6.

(4) Noodleman, L.; Norman, J. G.; Osborne, J. H.; Aizman, A.; Case, D. A. Models for ferredoxins: electronic structures of iron-sulfur clusters with one, two, and four iron atoms. *J. Am. Chem. Soc.* **1985**, *107* (12), 3418–3426 DOI: 10.1021/ja00298a004.

(5) Neese, F. Prediction of molecular properties and molecular spectroscopy with density functional theory: From fundamental theory to exchange-coupling. *Coord. Chem. Rev.* **2009**, *253* (5–6), 526–563 DOI: 10.1016/j.ccr.2008.05.014.

(6) Soda, T.; Kitagawa, Y.; Onishi, T.; Takano, Y.; Shigeta, Y.; Nagao, H.; Yoshioka, Y.; Yamaguchi, K. Ab initio computations of effective exchange integrals for H–H, H–He–H and Mn2O2 complex: comparison of broken-symmetry approaches. *Chem. Phys. Lett.* **2000**, *319* (3–4), 223–230 DOI: 10.1016/S0009-2614(00)00166-4.

(7) Grimme, S. Semiempirical GGA-type density functional constructed with a long-range dispersion correction. *J. Comput. Chem.* **2006**, *27* (15), 1787–1799 DOI: 10.1002/jcc.20495.

(8) Singh, M. K.; Rajaraman, G. Can CH···π interactions be used to design single-chain magnets? *Chem. - A Eur. J.* **2015**, *21* (3), 980–983 DOI: 10.1002/chem.201404853.

(9) Reinen, D.; Atanasov, M.; Köhler, P.; Babel, D. Jahn–Teller coupling and the influence of strain in Tg and Eg ground and excited states – A ligand field and DFT study on halide MIIIX6 model complexes [M = TiIII–CuIII; X = F−, Cl−]. *Coord. Chem. Rev.* **2010**, *254* (23–24), 2703–2754 DOI: 10.1016/J.CCR.2010.04.015.

Table S3. Transition energies (ΔE, cm^{-1}) and individual contributions of excited states to D and E ZFS parameters (cm^{-1}): for compound **1** (CASSCF(7, 5)+NEVPT2) (lowest 9 doublet and 9 quartet excited states)

Mult	Root	ΔE, cm^{-1}	D	E
4	0	0.0	0	0
4	1	2152.0	3.2	-2.8
4	2	2366.8	0.7	1.0
4	3	4403.4	18.3	17.9
4	4	5122.6	14.6	-14.2
4	5	11771.6	0.0	0.0
4	6	13339.5	0.0	0.0
4	7	19897.2	0.0	0.0
4	8	21871.1	0.1	-0.1
4	9	22181.7	0.1	0.1
2	0	12445.5	0.0	0.0
2	1	13882.9	0.0	0.0
2	2	17629.1	3.9	0.0
2	3	18563.6	0.0	0.0
2	4	19758.9	-1.0	0.9
2	5	20020.4	-1.5	-1.4
2	6	20528.8	-0.2	-0.1
2	7	20583.6	-0.6	0.6
2	8	20625.9	8.8	0.0
2	9	21932.3	0.0	0.0

Table S4. Transition energies (ΔE, cm^{-1}) and individual contributions of excited states to D and E ZFS parameters (cm^{-1}): for compound **2** (CASSCF(7, 5)+NEVPT2) (lowest 9 doublet and 9 quartet excited states)

Mult	Root	ΔE, cm^{-1}	D	E
4	0	0.0	0	0
4	1	2809.7	1.4	-0.7
4	2	2960.9	0.5	0.3
4	3	5070.4	16.3	14.6
4	4	5498.2	14.3	-13.0
4	5	13333.8	0.0	0.0
4	6	14562.6	0.0	0.0
4	7	20933.2	0.0	0.0
4	8	22623.2	0.2	-0.1
4	9	22789.8	0.2	0.1
2	0	12457.5	0.0	0.0
2	1	13598.2	0.0	0.0
2	2	17829.9	2.7	0.0
2	3	18472.2	0.0	0.0
2	4	20452.8	-1.2	0.4
2	5	20621.1	-1.5	-0.6
2	6	21120.1	-0.1	-0.1
2	7	21127.4	0.0	0.3
2	8	20599	10.1	0.0
2	9	22516.8	0.0	0.0

Table S5. Transition energies (ΔE, cm^{-1}) and individual contributions of excited states to D and E ZFS parameters (cm^{-1}): for compound **3** (CASSCF(5, 5)+NEVPT2)

Mult	Root	ΔE, cm^{-1}	D	E
6	0	0.0	0	0
4	0	18600.0	-0.9	-0.9
4	1	19090.5	-0.8	0.8
4	2	28172.3	0.0	0.0
4	3	28290.8	0.0	0.0
4	4	28858.4	0.0	0.0
4	5	29306.7	0.3	0.0
4	6	29925.3	0.0	0.0
4	7	30464.5	0.0	0.0
4	8	30605.3	0.0	0.0
4	9	32414.7	0.1	0.1
4	10	32682.6	0.0	0.0
4	11	34875.9	2.2	0.0
4	12	34891.3	0.0	0.0
4	13	35774.1	0.0	0.0
4	14	36375.8	0.0	0.0
4	15	43630.8	-0.7	0.7
4	16	44357.6	-0.7	-0.7
4	17	50074.1	0.0	0.0
4	18	50129.8	0.0	0.0
4	19	52057.9	0.0	0.0
4	20	52236.4	0.0	0.0
4	21	52324.4	0.0	0.0

4	22	55451.2	0.0	0.0
4	23	55919.8	0.0	0.0

Table S6. Transition energies (ΔE, cm^{-1}) and individual contributions of excited states to D and E ZFS parameters (cm^{-1}): for compound **5** (CASSCF(8, 5)+NEVPT2)

Mult	Root	ΔE, cm^{-1}	D	E
3	0	0.0	0	0
3	1	6712.3	-63.7	0.0
3	2	8179.0	24.5	-24.5
3	3	9755.2	20.7	20.7
3	4	14077.1	0.8	0.8
3	5	14673.9	0.7	-0.7
3	6	15232.9	0.0	0.0
3	7	26001.6	0.0	0.0
3	8	26586.6	0.0	0.0
3	9	28293.6	0.0	0.0
1	0	14965.3	0.0	0.0
1	1	16084.1	0.0	0.0
1	2	22355.8	16.4	0.0
1	3	23552.1	-7.2	7.2
1	4	24880.3	-6.6	-6.6
1	5	28124.8	0.0	0.0
1	6	29308.3	-0.2	-0.2
1	7	30120	-0.2	0.2
1	8	33145.9	0.0	0.0
1	9	35611.3	0.0	0.0
1	10	36210.9	1.8	0.0
1	11	36669.4	0.0	0.0
1	12	37072.5	-1.2	-1.2

1	13	37269.4	-1.0	-1.0
1	14	62860.7	0.0	0.0

Table S7. d-Orbitals splitting (cm^{-1}) according to AI-LFT analysis for complexes 1-3, 5

AOs	Co (**1**)	Co (**2**)	AOs	Fe (**3**)	AOs	Ni (**5**)
d_{yz}	0.0	0.0	0.54 d_{yz}+0.83 d_{xz}	0.0	d_{xy}	0.0
d_{xz}	220	191	0.84 d_{yz} -0.55 d_{xz}	64	d_{yz}	393
d_{xy}	2197	2863	$d_{x^2-y^2}$	5119	d_{xz}	725
$d_{x^2-y^2}$	3464	3907	d_{xy}	7377	$d_{x^2-y^2}$	5684
d_{z^2}	8600	9289	d_{z^2}	12336	d_{z^2}	9653

Table S8. Multi-determinant wave function of the ground and selected excited states for complexes **1**, **2**, **3** and **5** with heptacoordinated metal center. The computed CI states composition (in %, configurations with contribution larger than 10% are shown).

Compound 1, ground quartet state

	87%	13%
d_{z2}	1	1
d_{x2-y2}	1	2
d_{xy}	1	2
d_{xz}	2	1
d_{yz}	2	1

3rd excited quartet state

	52%	27%	22%
d_{z2}	1	2	1
d_{x2-y2}	2	1	1
d_{xy}	1	1	2
d_{xz}	2	2	1
d_{yz}	1	1	2

4th excited quartet state

	62%	24%	14%
d_{z2}	1	2	1
d_{x2-y2}	2	1	1
d_{xy}	1	1	2
d_{xz}	1	1	2
d_{yz}	2	2	1

9th excited doublet state

%	66%	11%
d_{z2}	1	1
d_{x2-y2}	2	2
d_{xy}	0	2
d_{xz}	2	2
d_{yz}	2	0

Compound 2, ground quartet state

	86%	13%
d_{z2}	1	1
d_{x2-y2}	1	2
d_{xy}	1	2
d_{xz}	2	1
d_{yz}	2	1

3rd excited quartet state

%	46%	26%	25%
d_{z2}	1	2	1
d_{x2-y2}	2	1	1
d_{xy}	1	1	2
d_{xz}	2	2	1
d_{yz}	1	1	2

4th excited quartet state

	56%	24%	18%
d_{z2}	1	2	1
d_{x2-y2}	2	1	1
d_{xy}	1	1	2
d_{xz}	1	1	2
d_{yz}	2	2	1

9th excited doublet state

%	58%
d_{z2}	1
d_{x2-y2}	2
d_{xy}	0
d_{xz}	2
d_{yz}	2

Compound 3, ground sextet state

	100%
d_{z2}	1
d_{xy}	1
d_{x2-y2}	1
d_{yz}	1
d_{xz}	1

1st excited quartet state

%	81%
d_{z2}	0
d_{xy}	1
d_{x2-y2}	1
d_{yz}	1
d_{xz}	2

2nd excited quartet state

	83%
d_{z2}	0
d_{xy}	1
d_{x2-y2}	1
d_{yz}	2
d_{xz}	1

12th excited quartet state

%	60%	13%	13%
d_{z2}	1	1	1
d_{xy}	2	0	1
d_{x2-y2}	0	2	1
d_{yz}	1	1	2
d_{xz}	1	1	0

16th excited quartet state

%	46%	25%	23%
d_{z2}	2	1	1
d_{xy}	1	1	2
d_{x2-y2}	1	2	1
d_{yz}	0	0	1
d_{xz}	1	1	0

17th excited quartet state

%	45%	26%	23%
d_{z2}	2	1	1
d_{xy}	1	1	2
d_{x2-y2}	1	2	1
d_{yz}	1	1	0
d_{xz}	0	0	1

Compound 5, ground state

	100%
d_{z2}	1
d_{x2-y2}	1
d_{yz}	2
d_{xz}	2
d_{xy}	2

1st excited triplet state

	100%
d_{z2}	1
d_{x2-y2}	2
d_{yz}	2
d_{xz}	2
d_{xy}	1

2nd excited triplet state

	56%	42%
d_{z2}	2	1
d_{x2-y2}	1	2
d_{yz}	1	1
d_{xz}	2	2
d_{xy}	2	2

3rd excited triplet state

	56%	42%
d_{z2}	2	1
d_{x2-y2}	1	2
d_{xy}	2	2
d_{xz}	1	1
d_{yz}	2	2